Geophysical Journal International

*Geophys. J. Int.* (2014) **197,** 1532–1536 doi: 10.1093/gji/ggu123

EXPRESS LETTER

# Geology, tectonics and topography underlined by L'Aquila earthquake TIR precursors

Luca Piroddi,[1] Gaetano Ranieri,[1] Friedemann Freund[2,3] and Antonio Trogu[1]

[1]*Department of Civil Engineering, Environmental Engineering and Architecture (DICAAR), University of Cagliari, Cagliari, Italy. E-mail: lucapiroddi@yahoo.it*
[2]*Earth Sci. Div., NASA Ames Research Center, Moffett Field, CA, USA*
[3]*Department of Physics, San Jose State University, San Jose, CA, USA*

Accepted 2014 March 31. Received 2014 March 28; in original form 2014 February 5

## SUMMARY

Anomalous thermal infrared (TIR) emissions have widely been detected by satellite sensors before the major earthquakes. A recent processing technique for geostationary thermal data, developed for the case of the 2009 April 6, magnitude 6.3 L'Aquila earthquake, makes it possible to identify areas of enhanced TIR emissions around the epicentral region at a mean distance of less than 50 km but inside a radius of about 100 km. The index, called Night Thermal Gradient (NTG), derived from 4-D time-series data (two spatial and two temporal coordinates), identifies TIR anomalies by following the temperature trend during night, when the surface of the Earth is expected to cool. Leading up to the L'Aquila earthquake, an anomalous warming trend was observed. In this study, the anomalous NTG pattern is compared to the expected normal trend, taking into account the seismogenic faults, the overall tectonic setting, lithological spatial features, the orography and world stress map near the epicentral region. Main results are that a certain lithological selectivity can be recognized and that the known main stress field and seismogenic faults seem to be less important than certain tectonic lineaments, which are classified as non-seismogenic. The strong correlation between the topography and the TIR anomalies is in agreement with proposed physical mechanism for the generation of TIR anomalies. This relation is, in turn, present mainly in correspondence to two tectonic lineaments which in particular are thrusts: therefore, strong compressive states seem to be a positive condition for the generation of TIR anomalies. The temporary modification of these stress fields have triggered the Paganica Fault to its normal rupture mechanism. It is important to note that the distances, over which the TIR anomalies occurred, are an order of magnitude larger than the estimated length of the main fault rupture. Pixel-by-pixel time-series comparisons between the maximum TIR anomaly area and the epicentre of the main shock show that the increase in radiative emission occurred in the areas of maximum TIR anomalies and did not start by spreading outward from the epicentral region.

**Key words:** Spatial analysis; Earthquake dynamics; Earthquake interaction, forecasting, and prediction; Dynamics: seismotectonics; Heat generation and transport; Fractures and faults.

## 1 INTRODUCTION

Using data from meteorological satellites, which derive ground surface temperatures from thermal infrared (TIR) measurements, many authors have reported over the past 20 yr on a correlation between apparent anomalous ground surface temperatures and impending earthquake activity (Gorny *et al.* 1988; Tramutoli *et al.* 2001; Tronin *et al.* 2002, 2004; Ouzounov & Freund 2004; Tramutoli *et al.* 2005; Ouzounov *et al.* 2007; Genzano *et al.* 2009; Wei *et al.* 2009; Tronin 2010; Piroddi & Ranieri 2011, 2012; Saraf *et al.* 2012; Wu *et al.* 2012, Qin *et al.* 2013).

Here, we present an in-depth analysis of TIR data related to the L'Aquila earthquake, 2009 April 6th (ML 5.9, $M_W$ 6.3, depth about 8.3 km), using a processing method recently developed to extract information from available high-frequency time-sequence TIR images (Piroddi 2011; Piroddi & Ranieri 2012). In the first analysis, a finite number of pixels surrounding the epicentre area were found to indicate an anomalous night-time increase

in the IR emission in the thermal IR window, interpreted as warming several nights before the main shock (Piroddi & Ranieri 2012). In this new study, a more detailed comparison is done between the observed TIR anomalies and the overall environmental settings.

In the earlier work (Piroddi & Ranieri 2012), TIR anomalies have been identified as possible precursors to the main shock. They appeared during the night of the 29th to 30th of March and reached maximum of intensities during the nights of the 2nd to 3rd and of the 3rd to 4th of April 2009, 3–2 d preceding the earthquake. Weaker TIR anomalies were observed on the night of the 6th to 7th April, one night after the earthquake.

The pattern of the thermal anomaly of the night from 3rd to 4th April here is compared with the main settings which could be important for the generation and diffusion of heat to the land surface. These environmental settings include lithological and topographic factors, known stress map, tectonic maps and the seismogenic faults distribution.

Furthermore, a time analysis is performed, through a time-series comparison of two pixels, one belonging to the maximum anomaly area and the other one containing the epicentre of the main shock, in order to put in evidence the dynamics of the thermal phenomenon dynamics, and if a thermal perturbation eventually started from the epicentre surface spreading to the areas of maximum anomaly amplitude or not.

## 2 THERMAL EARTHQUAKE ANOMALIES THEORIES

Anomalous satellite observations in TIR bands before and sometimes after the major earthquake have been widely reported as indicated in Section 1, and are explained by different generation mechanisms, the most frequently cited are:

- Greenhouse gas emission due to the dilatancy theory (Scholz *et al.* 1973), which are selective to the infrared (IR) radiation and cause temperature raising to reach radiative stability (Tronin 2010).
- Radon gas emission, mostly attributed to the same dilatancy theory, which leads to radioactive decay with high-energy emissions able to catalyse air humidity change and subsequent latent heat release (Pulinets *et al.* 2006).
- Activation of electronic charge carriers in minerals with semiconductor modality and propagation of these charge carriers to the ground surface where their recombination leads to IR emissions, spectrally distinct from grey body thermal emission, and also to air humidity changes (Freund 2003; Freund *et al.* 2007).

Other thermal sources have been presented in the literature but these are actually the most widely discussed. All have been demonstrated by laboratory or field data observations so that their action could generally be considered consistent, if confirmed for any single case.

## 3 NIGHT THERMAL GRADIENT: THERMAL DATA PROCESSING

A full discussion of the adopted thermal processing method, Night Thermal Gradient (NTG), can be found in its original definitions (Piroddi 2011; Piroddi & Ranieri 2012).

This method works on 4-D thermal data, two spatial and two temporal variables. It has been developed for geostationary satellite data starting from Land Surface Temperature (LST) data estimated and provided by the agency Satellite Application Facility on Land Surface Analysis (LSA SAF) of EUMETSAT consortium, based on acquisitions in the TIR channels of the SEVIRI sensor on Meteosat9.

LSA SAF algorithm for the estimation of LST is based on the split window method applied to the bands of 10.8 and 12.0 μm (Trigo *et al.* 2008):

$$\mathrm{LST} = \left(A_1 + A_2\frac{1-\varepsilon}{\varepsilon} + A_3\frac{\Delta\varepsilon}{\varepsilon^2}\right)\frac{T_{10.8}+T_{12.0}}{2} + \left(B_1 + B_2\frac{1-\varepsilon}{\varepsilon} + B_3\frac{\Delta\varepsilon}{\varepsilon^2}\right)\frac{T_{10.8}-T_{12.0}}{2} + C + \Delta\mathrm{LST},$$

where $\varepsilon$ is the mean emissivity and $\Delta\varepsilon$ the difference for the two spectral bands used. Other estimation parameters are the empirical coefficients of calibration with ground measures ($A_{1,2,3}$; $B_{1,2,3}$; $C$) and a correction based on the estimation of the instrumental error on the starting data ($\Delta$LST).

The NTG used to produce the thermal maps to be compared with environmental settings involves the processing of temporal data distributed throughout the night (41 samples, every 15 min from 18:00 to 4:00 UTC) and computing data from more nights (9 in the specific case) in order to reconstruct a virtual night (stack night).

The parameter chosen to monitor the thermal behaviour is the mean NTG obtained from a linear regression of the thermal data of each pixel for each stack night. In fact, to increase the signal-to-noise ratio and furthermore reduce the effects due to cloud cover, a moving average of the data in the correlation phase has been applied by means of a stack procedure with a processing window of 9 d. Linear interpolation procedure has been chosen with bisquare weights robustness constrains (DuMouchel & O'Brien 1989).

The representation of the NTG parameter is able to highlight areas where there is a night-time warming trend ($\mathrm{d}T/\mathrm{d}t > 0$), a phenomenon clearly abnormal compared to the behaviour of cooling and heat release in normal conditions at night (Piroddi & Ranieri 2012). Original geometrical resolution of maps for the observed areas corresponding to Central Italy ranges between 4 km (horizontal direction) and 5–6 km (vertical direction) because of the geostationary satellite projection.

The resulting parameters of interpolation are the intercept temperature ($T_0$) and NTG ($\mathrm{d}T/\mathrm{d}t$). The thermal analysis has been conducted with the parameter NTG ($\mathrm{d}T/\mathrm{d}t$), being this one the least affected by variable temperatures during the diurnal energization (Piroddi & Ranieri 2012).

The normal night-time trend of NTG is negative. Therefore, a thermal anomaly can be defined as positive values of NTG; in fact, night-time warming is in contradiction to the diurnal energization-release cycle and is indicative of an anomalous thermal phenomenon.

In most cases reported in the literature the observations are generally based on a single sample per day, usually at night, but occasionally using more night samples to highlight the temperature dynamics (Ouzounov *et al.* 2006; Bleier *et al.* 2009; Piroddi & Ranieri 2012).

## 4 RESULTS AND DISCUSSION

Looking at the tectonic layout of the areas surrounding L'Aquila, extracted from Cello (1997), a strong influence of the two nearest main thrust faults is immediately notable on the thermal patterns (Fig. 1a). In fact, the Olevano-Antrodoco line and the Gran Sasso thrust appear to have a dominant effect on of the two main thermal anomalies; a minimal thermal activity is observed inside the Gran Sasso unit which contains the most damaged city of L'Aquila (violet

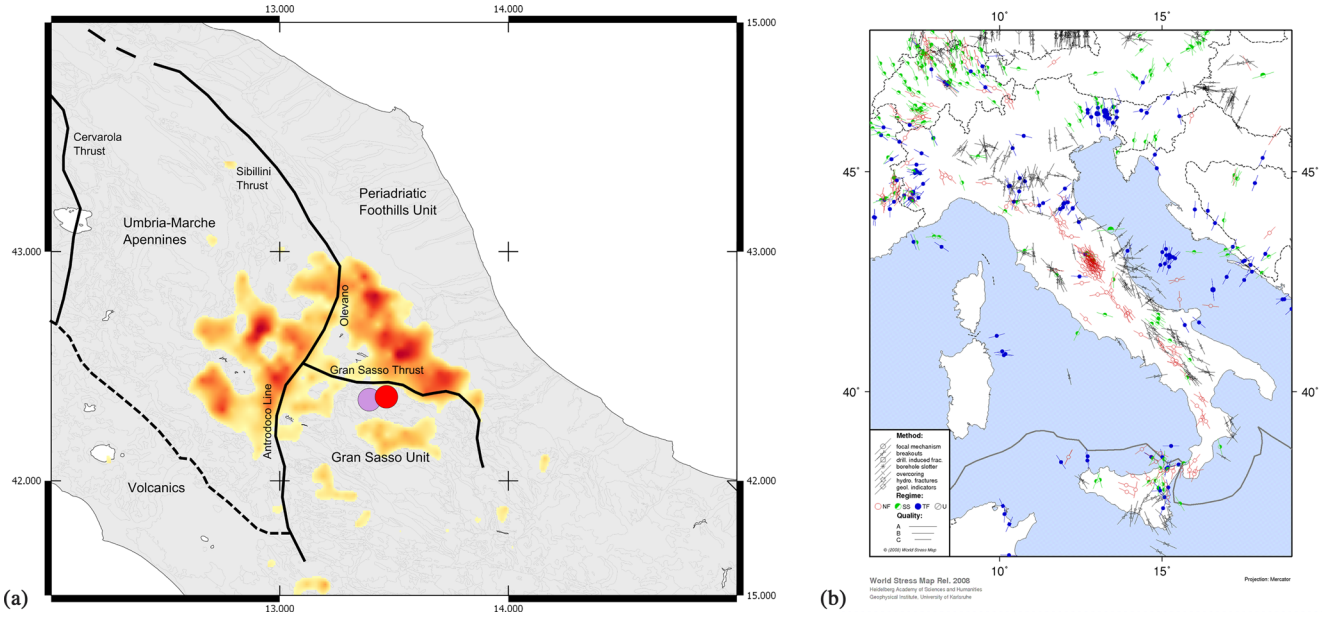


**Figure 1.** (a) Tectonic layout and thermal anomalies; (b) world stress map of Italy, with red for normal faults, blue for thrusts, green for strike-slip and black for unknown mechanism.

dot) and the Paganica (normal) Fault (red dot) that was activated during the main shock.

It is important to note that compressive lineaments actually are not indicated on the local World Stress Map (Heidbach *et al.* 2008). Instead, the entire median Apennines are shown as a succession of extensional normal faults, confining the compressive stress states to the borders of Italy near the Adriatic Sea and to the corresponding Balkan borders outside (Fig. 1b).

A further analysis can be done looking at the fault systems mapped by the national environmental agency Italian National Institute for Environmental Protection and Research (ISPRA). Through its online archives, it is possible to access two different data sets, a first one concerning the identification of the faults and geological discontinuities without regard for their seismogenic nature, and a second one which is called ITHACA (ITaly HAzard from CApable faults), containing only the faults considered candidates for considerable seismic events. A superimposition of these two faults data sets with the observed thermal anomalies is proposed in Fig. 2(a), where the main result is that the thermal anomalies are not directly associated with the seismogenic faults recognized in the ITHACA data set (blue lineaments). With respect to the assumed non-seismogenic fault systems (green lineaments), the two main thermal anomalies show a different distribution, one overlapping a dense fault system, while the second is located in an area indicated as free from faulting.

The lithological classification of the studied areas (Fig. 2b) indicates that the thermal anomaly associated with the most faulted area and with the Olevano-Antrodoco tectonic line is dominated by limestone formations, while the anomaly Eastern anomaly, near the Gran Sasso thrust in an area of only very low faults, is dominated by sandstone lithology.

To arrive at a more quantitative lithological response, a statistical analysis has been performed over the blue delimited areas of Fig. 2(b) covering a surface of about 40.620 km$^2$. This surface has

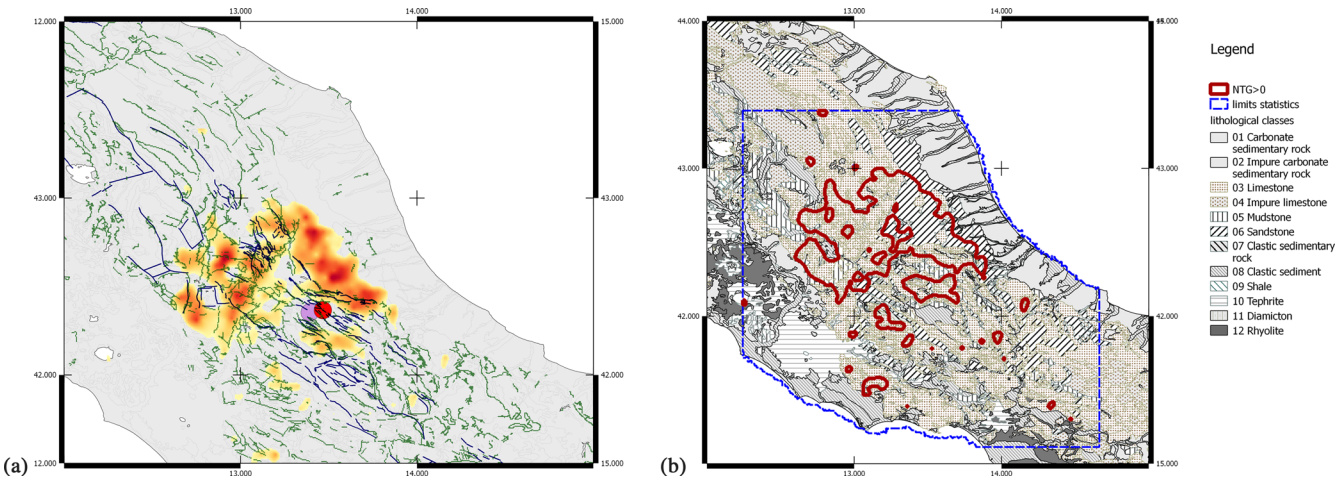


**Figure 2.** (a) Seismogenetic (blue) and non-classified fault systems (green) superimposed TIR anomalies; (b) superimposition of lithological classification with the borders of TIR anomaly areas.

**Table 1.** Statistics of lithological distribution in the overall area and in the anomalous areas.

| description | litho1 (area) [km$^2$] | NTG>0 (area) [km$^2$] | >0/litho1 | >0/>0tot | litho1/tot |
|---|---|---|---|---|---|
| Carbonate sedimentary rock | 3.379,0 | 47,2 | 1% | 1% | 8% |
| Clastic sediment | 6.885,4 | 326,8 | 5% | 5% | 17% |
| Clastic sedimentary rock | 141,8 | 51,3 | **36%** | 1% | 0% |
| Diamicton | 167,7 | 117,0 | **70%** | 2% | 0% |
| Dolomite | 16,5 | 0,0 | 0% | 0% | 0% |
| Impure carbonate sedimentary rock | 6,8 | 0,0 | 0% | 0% | 0% |
| Impure limestone | 999,2 | 19,2 | 2% | 0% | 2% |
| Limestone | 19.468,1 | 4.609,9 | **24%** | **76%** | **48%** |
| Mudstone | 2.852,2 | 546,6 | **19%** | 9% | 7% |
| rhyolite | 1.178,4 | 4,1 | 0% | 0% | 3% |
| Sandstone | 4.896,8 | 315,7 | 6% | 5% | 12% |
| Shale | 53,8 | 0,0 | 0% | 0% | 0% |
| Tephrite | 575,4 | 10,9 | 2% | 0% | 1% |
| Total | **40.621,1** | 6.048,7 | 15% | 100% | 100% |

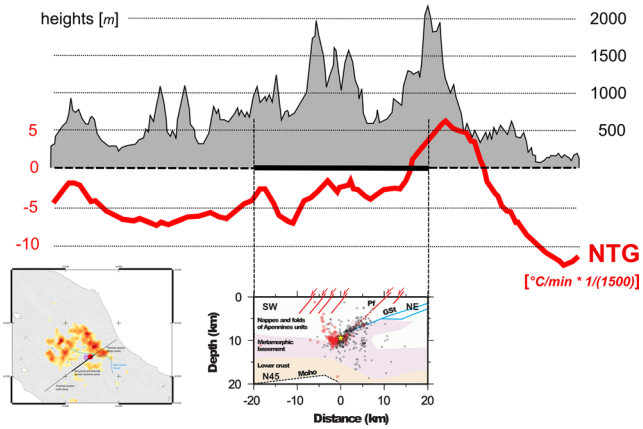


**Figure 3.** Tectonic section through the hypocentre with an elevation profile and a NTG profile.

been classified on the basis of the positive or negative values of the NTG index and the two components are measured and analysed (Table 1 and Fig. 3).

Looking at these statistical results, we note first that the Diamicton lithology has positive NTG values over 70 per cent of its extent (column '>0/litho1' in Table 1) but this range is small compared to the entire area (column 'litho1/tot' with a 0 per cent value) and to the whole positive NTG values area (column '>0/>0tot'). The Diamicton lithology is, in fact, rare in the region under study and mostly concentrated inside the anomalous areas. Similarly, clastic sedimentary rocks are represented in 36 per cent of their extent, but in very little total areas.

Looking at the differences between the areas with partial positive NTG values (compared to all positive areas) and the whole area we can point to a significant result: Limestone lithology, which covers 48 per cent of the whole area, covers 76 per cent of the positive NTG value areas. This result seems to arise mainly from the high proportion of limestone in the Olevano-Antrodoco area but also in part from southern anomaly near the epicentre which is more localized than the two major anomalies and also has lower NTG values, though still positive.

It is important to note that Limestone formations are typically regions of high exhalation rates of gases like $CO_2$, which is potentially an accessory cause to the thermal anomalies both through its nature as greenhouse gas and through the fact that it is a known Rn carrier gas (Petrini *et al.* 2012). However, the concept of electronic

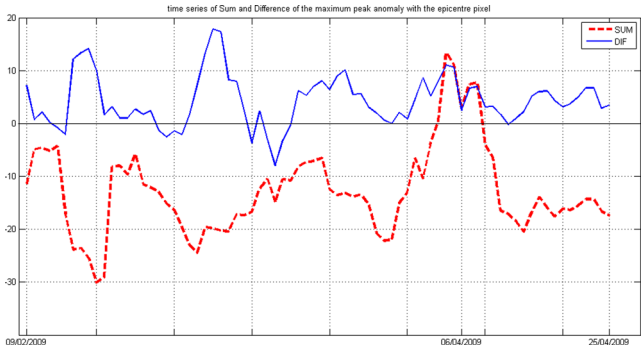


**Figure 4.** Time series of the sum and difference between the epicentre pixel and one of the peak maximal intensity pixels during the night of 2009 April 3. The horizontal axis give time in units of consecutive nights from February 9 to April 25 with the main shock on April 6 indicated by the thin vertical line.

charge carriers, stress-activated deep in the crust and propagating through the overlying rocks has recently been extended to this kind of lithology (Freund 2011).

A further analysis can be done looking at the fault dimension starting from the section through the hypocentre reported in Di Luccio *et al.* (2010). From this section (Fig. 3), it is possible to observe that the hypocentre (yellow star) is near the intersection of the Gran Sasso thrust (cyan) with the Paganica fault (red). The section also contains the main tectonic structures and minor seismicity hypocentres. By superimposing to this section, the graphs of the NTG distribution for the night of 3rd to 4th April (large red line) we clearly note the thermal activation of the Gran Sasso thrust, where low seismic activity was registered before the main shock (Di Luccio *et al.* 2010). Regarding the topographic profile, indicated by the black line and grey filling, we note that local maxima in topography are frequently associated with local maxima in NTG values.

The time-series comparison of two sets of pixels, one covering the maximum NTG anomaly area and the other the epicentre of the main shock, shows that there are nights when both the sum and the difference of the values calculated for each pixel increase but there are also other nights where the sum and the difference appear to be uncorrelated (Fig. 4). This suggests that the anomalous increase in TIR radiance occurred more selectively and more locally in areas of maximum anomalies and that the effect did not start at the epicentre, but was spreading outwards to the borders of the affected area in the form of a wave.

## 5 CONCLUSIONS

The main result of this analysis is that the pronounced TIR anomalies associated with the L'Aquila earthquake can be discussed in the context of the regional tectonic layout: two distinct thrusts are present near the TIR anomalies and seem to control their extent. It is noteworthy that according to fault catalogues and the world stress map, these thrusts are actually considered to have a low seismogenetic potential. However, they appear to have a strong influence on the TIR anomaly generation, which surround the seismogenetic fault systems that were activated in the L'Aquila event.

Another new insight has come from the lithological analysis, where one lithology, limestone, is more widely represented inside anomalous TIR areas than outside. This dominance of limestone over other lithographies is compatible with two models of gas

release, greenhouse gases and radon, as the cause of the TIR anomalies. It is also compatible, however, with the concept of electronic charge carriers, stress-activated deep below, which would be able to propagate through overlying limestone.

A topographic effect was definitely observed, in particular with regards to the cross-section through the hypocentre, which favours the theory of electric currents. This effect seems to be localized because the topographic heights nearest the two thrusts display the most pronounced TIR anomalies, while lesser TIR anomalies are observed at other topographic heights surrounding the epicentral area.

While the concurrent presence of more than one physical mechanism for the TIR anomalies origin is compatible with the observation, there seems to be a preference for electric currents spreading from the main thrusts to the immediate surrounding and the nearby topographic heights. These electric currents do not produce an actual temperature increase, but instead cause an increased radiance in the TIR region due to processes related to the recombination of the stress-activated electronic charge carriers coming from deep below (Freund *et al.* 2007).

Our analysis indicates that a large volume of rocks within the crust was probably subjected to considerable stress variations few days before the earthquake of 2009 April 6th and that the compressive nature of these forces created conditions that led to major TIR anomalies.

## ACKNOWLEDGEMENTS

Authors are grateful to Dr. Francesca Di Luccio for the schematics partially reported in Fig. 4. This material is reproduced with permission of John Wiley & Sons, Inc., © 2010. Authors gratefully acknowledge ISPRA agency for the cartographic data related to regional geology and fault systems.

F.T. Freund is supported by the NASA Earth Surface and Interior (ESI) Program, grant #NNX12AL71G.

## REFERENCES

Bleier, T., Dunson, C., Maniscalco, M., Bryant, N., Bambery, R. & Freund, F.T., 2009. Investigation of ULF magnetic pulsations, air conductivity changes, and infra red signatures associated with the 30 October 2007 Alum Rock M5.4 earthquake, *Nat. Hazards Earth Syst. Sci.,* **9,** 585–603.

Cello, G., 1997. Fractal analysis of a Quaternary fault array in the central Apennines, Italy, *J. Struct. Geol.,* **19**(I), 945–953.

Di Luccio, F., Ventura, G., Di Giovambattista, R., Piscini, A. & Cinti, F.R., 2010. Normal faults and thrusts reactivated by deep fluids: the 6 April 2009 Mw 6.3 L'Aquila earthquake, central Italy, *J. geophys. Res.,* **115,** B06315, doi:10.1029/2009JB007190.

DuMouchel, W. & O'Brien, F., 1989. Integrating a robust option into a multiple regression computing environment, in computing science and statistics, in *Proceedings of the 21st Symposium on the Interface,* pp. 297–301, eds Berk, K. & Malone, L., American Statistical Association.

Freund, F., 2003. Rocks that cranckle and sparkle and glow – strange pre-earthquake phenomena –, *J. Sci. Explor.,* **17,** 37–71.

Freund, F.T., 2011. Pre-earthquake signals: underlying physical processes, *J. Asian Earth Sci.,* **41,** 383–400.

Freund, F.T., Takeuchi, A., Lau, B.W.S., Al-Manaseer,, A., Fu, C.C., Bryant, N.A. & Ouzounov, D., 2007. Stimulated infrared emission from rocks: assessing a stress indicator, *eEarth,* **2,** 1–10.

Genzano, N *et al.*, 2009. RST analysis of MSG-SEVIRI TIR radiances at the time of the Abruzzo 6 April 2009 earthquake, *Nat. Hazards Earth Syst. Sci.,* **9**(6), 2073–2084.

Gorny, V.I., Salman, A.G., Tronin, A.A. & Shilin, B.B., 1988. The earth's outgoing IR radiation as an indicator of seismic activity, *Proc. Acad. Sci. USSR,* **301,** 67–69.

Heidbach, O., Tingay, M., Barth, A., Reinecker, J., Kurfeß, D. & Müller, B., 2008. *The World Stress Map database release,* doi:10.1594/GFZ.WSM.Rel2008.

Ouzounov, D. & Freund, F., 2004. Mid-infrared emission prior to strong earthquakes analyzed by remote sensing data, *Adv. Space Res.,* **33**(3), 268–273.

Ouzounov, D., Bryant, N., Logan, T., Pulinets, S. & Taylor, P., 2006. Satellite thermal IR phenomena associated with some of the major earthquakes in 1999–2003, *Phys. Chem. Earth A/B/C,* **31**(4–9), 154–163.

Ouzounov, D., Liu, D., Kang, C., Cervone, G., Kafatos, M. & Taylor, P., 2007. Outgoing long wave radiation variability from IR satellite data prior to major earthquakes, *Tectonophysics,* **431**(1–4), 211–220.

Petrini, R., Italiano, F., Riggio, A., Slejko, F.F., Santulin, M., Buccianti, A., Bonfanti, P. & Slejko, D., 2012. Coupling geochemical and geophysical signatures to constrain strain changes along thrust faults, *Boll. Geofis. Teorol. Appl.,* **53**(1), 113–134.

Piroddi, L., 2011. Sistemi di telerilevamento termico per il monitoraggio e la prevenzione dei rischi naturali: il caso sismico, *PhD thesis*, University of Cagliari, Available at: http://veprints.unica.it/550/ (last accessed 16 April 2014).

Piroddi, L. & Ranieri, G., 2011. Can the thermal remote sensing survey be considered as an earthquake precursor? *Environ. Semeiotics,* **4**(1), 1–9.

Piroddi, L. & Ranieri, G., 2012. Night thermal gradient: a new potential tool for earthquake precursors studies. An application to the seismic area of L'Aquila (central Italy), *IEEE J. Sel. Topics Appl. Earth Observ. Remote Sens. – JSTARS,* **5**(1), 307–312.

Pulinets, S.A., Ouzounov, D., Karelin, A.V., Boyarchuk, K.A. & Pokhmelnykh, L.A., 2006. The physical nature of thermal anomalies observed before strong earthquakes, *Phys. Chem. Earth A/B/C,* **31**(4–9), 143–153.

Qin, K., Wu, L., Zheng, S. & Liu, S., 2013. A deviation-time-space-thermal (DTS-T) method for global earth observation system of systems (GEOSS)-based earthquake anomaly recognition: criterions and quantify indices, *Remote Sens.* **5**(10), 5143–5151.

Saraf, A.K., Rawat, J.D.V., Mohammed, Z. & Kanika, S., 2012. Satellite detection of thermal precursors of Yamnotri, Ravar and Dalbandin earthquakes, *Nat. Hazards,* **61,** 861–872.

Scholz, C.H., Syke, L.R. & Aggarwal, Y.P., 1973. Earthquake prediction: a physical basis, *Science,* **181,** 803–809.

Tramutoli, V., Cuomo, V., Filizzola, C., Pergola, N. & Pietrapertosa, C., 2005. Assessing the potential of thermal infrared satellite survey for monitoring seismically active areas: the case of Kocaeli (Izmit) earthquake, August 17, 1999, *Remote Sens. Environ.,* **96,** 409–426.

Tramutoli, V., Di Bello, G. & Pergola, N., 2001. Robust satellite techniques for remote sensing of seismically active areas. *Ann. Geophys.,* **44**(2), 295–312.

Trigo, I.F., Monteiro, I.T., Olesen, F. & Kabsch, E., 2008. An assessment of remotely sensed land surface temperature, *J. geophys. Res.,* **113,** D17108, doi:10.1029/2008JD010035.

Tronin, A.A., Hayakawa, M. & Molchanov, O.A., 2002. Thermal IR satellite data application for earthquake research in Japan and China, *J. Geodyn.,* **33,** 519–534.

Tronin, A.A., Biagi, P.F., Molchanov, O.A., Khatkevich, Y.M. & Gordeev, E.I., 2004. Temperature variations related to earthquakes from observation at the ground stations and by satellites in Kamchatka area, *Phys. Chem. Earth,* **29,** 501–506.

Tronin, A.A., 2010. Satellite remote sensing in seismology. A review, *Remote Sens.,* **2**, 124–150.

Wei, L., Guo, J., Liu, J., Lu, Z., Li, H. & Cai, H., 2009. Satellite thermal infrared earthquake precursor to the Wenchuan MS 8.0 Earthquake in Sichuan, China, and its analysis on geo-dynamics, *Acta Geol. Sinica,* **83**(4), 767–775.

Wu, L., Qin, K. & Liu, S., 2012. GEOSS-based thermal parameters analysis for earthquake anomaly recognition, *Proc. IEEE,* **100**(10), 2891–2907.